The Astrophysical Journal, 934:118 (11pp), 2022 August 1 https://doi.org/10.3847/1538-4357/ac6ce5

Exploring the Hadronic Origin of LHAASO J1908+0621

Agnibha De Sarkar and Nayantara Gupta
Astronomy & Astrophysics group, Raman Research Institute, C. V. Raman Avenue, 5th Cross Road, Sadashivanagar, Bengaluru 560080, Karnataka, India
agnibha@rri.res.in
Received 2022 January 13; revised 2022 May 3; accepted 2022 May 3; published 2022 July 29

Abstract

Recent observations by the Large High Altitude Air Shower Observatory (LHAASO) have paved the way for the observational detection of PeVatrons in the Milky Way, thus revolutionizing the field of γ-ray astrophysics. In this paper, we study one such detected source, LHAASO J1908+0621, and explore the origin of multi-TeV γ-ray emission from this source. A middle-aged radio supernova remnant SNR G40.5–0.5 and a GeV pulsar PSR J1907+0602 are cospatial with LHAASO J1908+0621. Dense molecular clouds are also found to be associated with SNR G40.5–0.5. We explain the multi-TeV γ-ray emission observed from the direction of LHAASO J1908+0621, by the hadronic interaction between accelerated protons that escaped from the SNR shock front and cold protons present inside the dense molecular clouds, and the leptonic emission from the pulsar wind nebula (PWN) associated with the pulsar J1907+0602. Moreover, we explain lower energy γ-ray emission by considering the radiative cooling of the electrons that escaped from SNR G40.5–0.5. Finally, the combined lepto-hadronic scenario was used to explain the multiwavelength spectral energy distribution of LHAASO J1908+0621. Although not yet significant, an IceCube hotspot of neutrino emission is spatially associated with LHAASO J1908+0621, indicating a possible hadronic contribution. In this paper, we show that if a hadronic component is present in LHAASO J1908+0621, then the second-generation IceCube observatory will detect neutrinos from this source.

Unified Astronomy Thesaurus concepts: High energy astrophysics (739); Gamma-ray sources (633); Gamma-rays (637); Supernova remnants (1667); Molecular clouds (1072)

1. Introduction

Cosmic rays (CR) are charged atomic nuclei, traversing through space with relativistic speed. The CRs consist of 90% protons, about 8%–9% helium nuclei, and smaller abundances of heavier elements. The observed local proton spectrum can be well described by a single power law with an index of -2.7, up to around 1 PeV ($=10^{15}$ eV) energy, which is also known as the "knee" of the CR spectrum. This hints toward the presence of powerful astrophysical proton accelerators in our Galaxy, which can accelerate the CR protons to PeV energies, the so-called "PeVatrons." Despite having been theoretically studied very thoroughly, no Galactic source has been unambiguously confirmed to be a PeVatron, except the possible case of the Galactic center (H.E.S.S. Collaboration et al. 2016, 2018; MAGIC Collaboration et al. 2020). Since CRs, which can accelerate up to PeV energies, can interact with an ambient medium to produce multi-TeV energy γ-rays, the PeVatrons can be identified by studying the association of γ-ray sources with them. To that end, successful operations by ground-based observatories such as the High Energy Stereoscopic System (H.E.S.S.)[1], Major Atmospheric Gamma Imaging Cherenkov (MAGIC)[2], Tibet ASγ[3] https://www.icrr.u-tokyo.ac.jp/em/index.html, High-Altitude Water Cherenkov (HAWC)[4], and the Large High Altitude Air Shower Observatory (LHAASO)[5] over the past ten years have made the ultra-high-energy (UHE) γ-ray astronomy an active area of research. Since the UHE γ-rays produced outside our Galaxy get heavily attenuated by the cosmic microwave background (CMB) and infrared background (IRB), it is difficult to detect UHE γ-ray sources outside our Galaxy. However, the recent detections of many γ-ray sources, emitting γ-rays with energies ranging from several hundreds of TeV to PeV, have increased the possibilities to unambiguously confirm the presence of PeVatrons residing in our Galaxy.

LHAASO is a state-of-the-art dual-task facility designed for CRs and γ-ray studies at a few hundred GeV to a few PeV, located at 4410 m above sea level in China (Cao 2010). Since starting its operation in 2020 April, LHAASO has detected more than a dozen of UHE γ-ray sources in our Galaxy. Many of these sources are associated with PWNe or supernova remnants (SNRs). Since the LHAASO observatory is sensitive enough to detect UHE γ-rays coming from a source, the chances of establishing astrophysical sources such as PWN or SNR as possible PeVatrons are very strong. For this work, we study one of such UHE γ-ray sources observed by LHAASO, which has a strong possibility of being a Galactic PeVatron (Cao et al. 2021).

LHAASO J1908+0621 is a UHE γ-ray source, detected in a serendipitous search for γ-ray sources by the LHAASO observatory (Cao et al. 2021). This source was detected with 12 other sources with energies $\geqslant 100$ TeV and statistical significance $\geqslant 7\sigma$. The LHAASO source is located at R. A. $= 287.^{\circ}05$ and decl. $= 6.^{\circ}35$, with a significance above 100 TeV to be 17.2σ, making it one of the brightest UHE γ-ray sources in our Galaxy. The γ-ray spectrum of this source reaches up to a maximum energy of 0.44 ± 0.05 PeV, and the differential photon flux of this source at 100 TeV was found to be 1.36 ± 0.18 Crab Unit (Crab Unit = flux of the Crab Nebula

[1] https://www.mpi-hd.mpg.de/hfm/HESS/
[2] https://magic.mpp.mpg.de
[4] https://www.hawc-observatory.org
[5] http://english.ihep.cas.cn/lhaaso/

at 100 TeV, 1 Crab Unit $= 6.1 \times 10^{-17}$ photons $\mathrm{TeV}^{-1}\,\mathrm{cm}^{-2}\,\mathrm{s}^{-1}$). Because the maximum energy that the UHE γ-rays emitted from LHAASO J1908+0621 can attain is greater than 100 TeV, this source shows a strong possibility of being associated with a Galactic PeVatron.

Cao et al. (2021) have obtained and fitted the γ-ray spectrum of LHAASO J1908+0621 with a simple power-law model and a log-parabola model. The log-parabola model gives a better fit compared to a simple power-law model, due to a gradual steepening of the γ-ray spectrum between 10 TeV and 500 TeV. Although this steepening can be due to γ-ray absorption from background photons, the effect of absorption was found to be small, even at very high energies. The best-fit parameters for the log-parabola γ-ray spectral fit of LHAASO J1908 +0621 are $a = 2.27$ and $b = 0.46$, where the log-parabola model is defined by $(E/10\,\mathrm{TeV})^{-a-b\,\log(E/10\,\mathrm{TeV})}$. The 68% contamination angle for LHAASO J1908+0621 was found to be $0.^{\circ}45$, obtained for γ-rays over 25 TeV. HAWC observatory has observed the LHAASO source to have a hard spectrum reaching energies above 100 TeV without any hint of an exponential cutoff, making it the best case for Galactic PeVatrons (HAWC Collaboration et al. 2019). This source was first observed by the MILAGRO observatory (Abdo et al. 2007) and was later confirmed by the H.E.S.S. observatory (Aharonian et al. 2009), which detected the source with a large angular size ($\sigma = 0.^{\circ}34$) and a hard spectral index of 2.1, above 300 GeV. ARGO-YBJ observatory (Astrophysical Radiation with Ground-based Observatory at YangBaJing; Bartoli et al. 2012) has found that the TeV luminosity of this source is comparable to the Crab Nebula, which makes it one of the most luminous Galactic γ-ray sources in the TeV regime. The observation by the Very Energetic Radiation Imaging Telescope Array System (VERITAS); Aliu et al. 2014) observatory has also revealed an extended source system ($\sigma = 0.^{\circ}44$), with three peaks of emission and also, a photon index of 2.2. Additionally, the LHAASO source is associated with an IceCube neutrino hotspot, although the significance is low (Aartsen et al. 2019a, 2020). The extended nature of the LHAASO source indicates that an SNR and/or PWN should be associated with this source. To that end, the study of possible counterparts of LHAASO J1908+0621 is necessary to establish both the γ-ray production region and nearby particle accelerators.

LHAASO J1908+0621 is spatially associated with a middle-aged, shell-type supernova remnant SNR G40.5–0.5 (20–40 kyr; Downes et al. 1980), which is brighter in the northern region of the TeV source, as observed in the radio data obtained by VLA Galactic Plane Survey (VGPS; Stil et al. 2006). The distance estimation places the SNR at a distance of 3.5 kpc, by CO observations (Yang et al. 2006) or a more distant position of 5.5–8.5 kpc, using the Σ–D relation (Downes et al. 1980) and 6.1 kpc (Case & Bhattacharya 1998). The recently discovered relatively young and energetic radio pulsar PSR J1907+0631 (characteristic age $\tau = 11$ kyr, spin-down luminosity $\sim 5 \times 10^{35}\,\mathrm{erg\,s}^{-1}$) lies close to the projected center of the SNR (Lyne et al. 2017). The estimated distance of this pulsar obtained from the dispersion measure (DM) is 7.9 kpc, which is compatible with the estimated distance of G40.5–0.5 and hints toward an association between these two objects. Although in principle, PSR J1907+0631 can power the entire TeV source (Duvidovich et al. 2020), the considerable offset between the pulsar and the position of the γ-ray emission disfavors that scenario. Additionally, the distribution of molecular clouds (MCs) has been confirmed from studies involving the distribution of CO gas in the vicinity of SNR G40.5–0.5. Li et al. (2021) have searched for MCs with ^{12}CO ($J = 1$–0), ^{13}CO ($J = 1$–0), and C^{18}O ($J = 1$–0) emission lines, and discovered the MCs to be spatially associated with SNR G40.5–0.5 in the ^{12}CO ($J = 1$–0) and ^{13}CO ($J = 1$–0) maps between the integrated velocity range of 46 and 66 km s^{-1}. A shell-like cavity around the radio morphology of SNR G40.5–0.5 was also observed in the ^{12}CO ($J = 1$–0) and ^{13}CO ($J = 1$–0) maps, indicating a possible SNR swept-up shell (Li et al. 2021). The presence of MCs is also confirmed by Crestan et al. (2021), in which they were discovered in the ^{12}CO ($J = 1$–0) and ^{13}CO ($J = 1$–0) maps in the velocity range of 58–62 km s^{-1}. This discovery places the SNR+MC association at a near distance of ~3–3.5 kpc and far distance of ~8–9.5 kpc, and the corresponding mean number density of the MCs were estimated to be 110–180 cm^{-3} assuming near distance and 45-60 cm^{-3} assuming far distance (Li et al. 2021; Crestan et al. 2021).

Apart from the SNR G40.5–0.5 and PSR J1907+0631, a γ-ray loud pulsar, PSR J1907+0602, was also found to be spatially associated with LHAASO J1908+0621, located in the southern part of the source (Crestan et al. 2021). The pulsar has a characteristic age of 19.5 kyr and a spin-down luminosity of $2.8 \times 10^{36}\,\mathrm{erg\,s}^{-1}$ (Abdo et al. 2010). The distance of the pulsar, estimated from DM, was found to be 3.2 ± 0.6 kpc (Abdo et al. 2010). Li et al. (2021) performed an off-pulse analysis of the Fermi-LAT data of the GeV pulsar PSR J1907 +0602 and discovered a previously undetected, extended source spatially associated with the MILAGRO counterpart of LHAASO J1908+0621, labeled as Fermi J1906+0626. Additionally, another unidentified GeV source 4FGL J1906.2 +0631, distance unknown, was located within the positional error of LHAASO J1908+0621 (Abdollahi et al. 2020).

Due to its complex spatial morphology, the origin of the γ-ray emission from LHAASO J1908+0621 is uncertain. Leptonic emission from PWN associated with PSR J1907 +0602 can be a possible origin of the multi-TeV γ-ray detected by LHAASO. The electrons can be accelerated up to 1 PeV at the wind termination shock of the PWN. However, electrons being leptons, lose energy radiatively very fast. Thus escape from the acceleration site and then further propagation can pose a real challenge to the scenario (Cao et al. 2021). Furthermore, if electrons are the progenitor of the γ-ray emission, no neutrinos should be detected by IceCube from the source region and the neutrino hotspot could not be explained. Alternatively, escaped protons from the shock of the SNR G40.5–0.5 can penetrate the associated MCs and through hadronic interaction, produce multi-TeV γ-rays. Although the SNR itself is too old to produce multi-TeV γ-rays, protons accelerated at earlier epochs can initiate high energy γ-ray emissions from the MC region (Cao et al. 2021). Moreover, in the hadronic scenario, one can also explain the neutrino hotspot near the source region. Intrigued by this fact, in this work, we explore the hadronic origin of LHAASO J1908+0621. We try to see the conditions in which the emission from the LHAASO source can be explained by γ-rays originating from p–p interaction between accelerated protons from the SNR and cold protons inside the MCs, as well as calculate the corresponding neutrino emission from the hadronic interaction and compare it to the sensitivity of the IceCube-Gen2 observatory (Aartsen

et al. 2019b). Additionally, we also consider leptonic emission from the PWN associated with PSR J1907+0602, as well as the leptonic emission from the SNR+MC system, along with the hadronic contribution, to understand the radiation mechanism implied by the observed multiwavelength (MWL) spectral energy distribution (SED).

In Section 2, we discuss the morphology of the complicated region surrounding LHAASO J1908+0621. In Section 3, we calculate the multi-TeV γ-ray emission through hadronic interaction between accelerated protons from SNR and cold protons residing in the MCs. In Section 4, we calculate the leptonic contributions from both SNR G40.5–0.5 and PWN associated with PSR J1907+0602. In Section 5, we calculate the corresponding neutrino SED from the hadronic interaction and compare the calculation with the sensitivity of the IceCube observatory. In Section 6, we discuss the obtained results, and in Section 7, we conclude this work.

2. Morphology

Detailed morphological study of the region surrounding LHAASO J1908+0621 has been reported by Li et al. (2021); Crestan et al. (2021) and Cao et al. (2021), using various observations by space-based and ground-based observatories. Through detailed Fermi-LAT data analysis, Li et al. (2021) have reported the position of the PWN associated with PSR J1907+0602. The position of SNR G40.5–0.5 and the surrounding MCs were also confirmed by radio observations and CO mapping respectively (Li et al. 2021; Crestan et al. 2021). In general, a clear separation of high energy radiation from the low energy emission, attributed to their different original objects, must be strongly supported by the morphological observation of the extended source, in which the objects are spatially well separated. However, due to the complex juxtaposition of potential counterparts along the line of sight of LHAASO J1908+0621, it is difficult to distinguish between the sources responsible for high energy and low energy emissions from the region. In this section, we discuss the emission mechanisms considered in this paper, to explain the MWL SED of LHAASO J1908+0621, while being consistent with the observed energy morphology of the source region.

Ground-based observatories, such as H.E.S.S. and VERITAS have good enough angular resolutions ($\sim 0\overset{\circ}{.}06$) to extract a high energy emission region in the direction of the LHAASO source. Although the significance is not very high, the significance map derived from the VERITAS observation indicates that the PWN associated with PSR J1907+0602 could be an important source for the very-high-energy (VHE; $E > 100$ GeV) γ-ray emission (Aliu et al. 2014; Li et al. 2021; Crestan et al. 2021). However, as given in Crestan et al. (2021), although the VERITAS emission lobe obtained from the significance map (significance levels ranging from 3σ to 5.2σ), matches well with the proposed PWN position, there is another VERITAS emission lobe, which is spatially coincident with the contact point between SNR G40.5–0.5 and the surrounding MCs (see Figure 1 and 3 of Crestan et al. 2021). This indicates that VHE γ-rays obtained from both PWN J1907+0602 and the SNR+MC system should contribute to the SED obtained by VERITAS. Similar to VERITAS, in the H.E.S.S. significance map obtained by H.E.S.S. Galactic Plane Survey (HGPS; Abdalla et al. 2018), emission lobes were found to be coincident with the position of PWN J1907+0602, as well as the contact region of the SNR+MC system. Moreover, the 68% containment region of the Gaussian morphology measured by H.E.S.S., comfortably overlaps with the SNR+MC system, as well as the PWN. The fact that the H.E.S.S. energy morphology contains two emission lobes spatially attributed to the VHE γ-ray radiation from both the PWN and the SNR +MC system, suggests that emissions from both the PWN and the SNR+MC system should be responsible for the VHE γ-ray data observed by H.E.S.S (Aharonian et al. 2009; Abdalla et al. 2018). This is why we have considered the contributions from both PWN J1907+0602 and the SNR+MC system to satisfy the VHE SEDs obtained from VERITAS and H.E.S.S. observations. We note that since the field of view (FOV) of the VERITAS observatory (FOV $\sim 3\overset{\circ}{.}5$; Galante 2012) is smaller than that of the H.E.S.S. observatory (FOV $\sim 5^{\circ}$; De Naurois 2019), VERITAS underestimates the total flux observed from the source region, as compared to that measured by the H.E.S.S. observatory. We have taken this into account while constructing the MWL SED of the source, and we have scaled the VERITAS SED to match that measured by the H.E.S.S. observatory.

For other ground-based observatories such as LHAASO and HAWC, the angular resolution may not be enough to draw a detailed morphological map of the source region, but it should be enough to establish the extent of high energy emission from the source region. Cao et al. (2021) have provided a KM2A significance map, which shows the potential counterparts of the UHE (>100 TeV) γ-ray source. From the inset of the extended data in Figure 5 of Cao et al. (2021), it can be seen that, similar to H.E.S.S., the reported PWN position given by Li et al. (2021) is within the extent of the UHE emission observed by LHAASO, although an offset of $0\overset{\circ}{.}18$, or 10 pc (at 3.2 kpc), is also present between the centroid of the LHAASO emission morphology and the best-fit position of the disk morphology used to explain the PWN in Li et al. (2021). On the other hand, the overlapping region of SNR G40.5–0.5 and the surrounding MCs is also situated well within the maximum significance region observed by LHAASO; however, the centroid of the UHE emission morphology observed by LHAASO, is also not coincident with the contact region between SNR G40.5–0.5 and the associated MCs. No distinct lobes of emission, like in the cases of H.E.S.S. and VERITAS, were found in the source morphology observed by LHAASO, making it difficult to ascertain which source, the PWN or the SNR+MC system, is actually contributing to the UHE regime. HAWC Collaboration et al. (2022) have tried to explain the UHE γ-ray data observed by LHAASO using one-zone and two-zone, purely leptonic scenarios originating from PWN J1907+0602. However, it was found that the corresponding synchrotron fluxes obtained from the proposed models exceed the X-ray upper limits measured by the XMM-Newton observatory (HAWC Collaboration et al. 2022). Consequently, in this work we explore the contribution of the SNR+MC system, which is another possible candidate overlapped with the image of LHAASO J1908+0621 (Cao et al. 2021), and determine the conditions for which the SNR +MC system would be responsible for the UHE γ-ray emission observed by LHAASO. The phenomenological model explored in this paper does not violate the observed X-ray upper limits.

As stated earlier, Li et al. (2021) discovered an extended source by performing Fermi-LAT data analysis during the off-peak phases of the PSR J1907+0602. They have shown that this extended source, Fermi J1906+0626, shows a significant peak coincident with the molecular material distribution

obtained from the CO mapping. This clearly implies that Fermi J1906+0626 is a result of interaction between accelerated particles from SNR G40.5–0.5 and the associated MCs. Moreover, as seen in Figure 2 of Li et al. (2021), the significance peak of Fermi J1906+0626 in the 0.1–2 GeV energy range is outside of the TeV significance contours presented by VERITAS, as well as the UHE emission morphology of LHAASO. So in this work, we explain the lower energy emission from the direction of LHAASO J1908 +0621 by the leptonic interaction between escaped electrons from the SNR shock front and the molecular material. Since inside MCs bremsstrahlung radiation will dominate IC cooling, due to enhanced material number density, we have explained the lower energy γ-ray SED (0.1–10GeV) using bremsstrahlung emission in the present work. Below, we discuss the theoretical framework of our model, used to explain the MWL SED of LHAASO J1908+0621.

3. Hadronic Modeling

In this section, we calculate the hadronic contribution to the total γ-ray flux observed by LHAASO from LHAASO J1908 +0621. The hadronic component comprises the γ-ray produced from the interaction between escaped protons from SNR G40.5–0.5 and cold protons residing inside the associated MCs. We assume that the SNR and MCs are at a distance of 8 kpc from the Earth, similar to Li et al. (2021). For that distance, the number density of the associated MCs was assumed to be 45 cm^{-3} (Li et al. 2021). As evident by the radio observations, the SNR shows a shell-like structure, outside of which the MCs are present. Due to this fact, we assumed that the supernova exploded at the center of the cavity of the shell that is surrounded by MCs, similar to Fujita et al. (2009). After the explosion, the shock expands inside the cavity and finally hits the surrounding MCs, which are assumed to be ~22 pc from the cavity center.

After the explosion, the supernova is in the free expansion phase, in which the ejecta from the explosion expands freely without any deceleration. After time $t_{\rm Sedov}$, the supernova enters the adiabatic Sedov phase, in which the mass of the swept-up interstellar medium (ISM) material by the shock wave increases and reaches densities that impede the free expansion. Rayleigh–Taylor instabilities arise once the mass of the swept-up ISM approaches that of the ejected material. In this phase, the cooling timescales are essentially much longer than the dynamical timescales, which makes this phase adiabatic in nature. This phase lasts until $t_{\rm Rad}$, after which the supernova enters the radiative phase. When the shock expands through various phases of supernova evolution, its radius and velocity change with time. The time dependence of shock velocity is given by Ohira et al. (2012); Fujita et al. (2009),

$$v_{\rm sh}(t) = \begin{cases} v_i & (t < t_{\rm Sedov}) \\ v_i (t/t_{\rm Sedov})^{-3/5} & (t_{\rm Sedov} < t) \end{cases} \quad (1)$$

where $v_{\rm sh}$ is the velocity of the shock and v_i denotes the initial velocity of the ejecta. We assume $v_i = 10^9$ cm s^{-1} (Fujita et al. 2009). We can obtain the time dependence of the shock radius by integrating Equation (1).

$$R_{\rm sh}(t) \propto \begin{cases} (t/t_{\rm Sedov}) & (t < t_{\rm Sedov}) \\ (t/t_{\rm Sedov})^{2/5} & (t_{\rm Sedov} < t) \end{cases}. \quad (2)$$

For this work, we assume the radius of the shock and time at the beginning of the Sedov phase, $R_{\rm Sedov}$ and $t_{\rm Sedov}$, to be 2.1 pc and 210 yr following Ohira et al. (2011); Makino et al. (2019).

The CR protons are accelerated through the diffusive shock acceleration (DSA) mechanism when the supernova is in the Sedov phase. The CRs are scattered back and forth across the shock front by magnetic turbulence during the acceleration as the shock front is expanding toward the surrounding MCs. Following Ohira et al. (2012) and Makino et al. (2019), we assume CR protons need to cross an escape boundary outside the shock front to escape from the SNR. To that end, we assume a geometrical confinement condition $l_{\rm esc} = \kappa R_{\rm sh}$ and adopt $\kappa = 0.04$ (Makino et al. 2019), where $l_{\rm esc}$ is the distance of the escape boundary from the shock front. Using this definition and Equation (2), we can write the escaping radius,

$$R_{\rm esc}(t) = (1 + \kappa) R_{\rm sh}(t), \quad (3)$$

.and we assume that the accelerated CR protons need to cross this escaping radius to contribute to further astrophysical processes.

After traversing through the cavity, the SNR shock eventually hits the surrounding MCs. The shock has to travel a distance of ~22 pc (=$r_{\rm MC}$, distance of the MCs from the cavity center) to collide with the MCs. Setting $R_{\rm esc} = r_{\rm MC}$, from Equations (2) and (3), the time of the collision can be found to be $t_{\rm coll} \sim 7.5 \times 10^3$ yr. Using $t_{\rm coll}$ in Equation (1), the velocity of the shock at the point of collision can be calculated to be $v_{\rm sh}(t_{\rm coll}) \sim 1.2 \times 10^8$ cm s^{-1}. Following Fujita et al. (2009), we assume the SNR is at the end of the Sedov phase at $t = t_{\rm coll}$, so the particle acceleration stops at $t \sim t_{\rm coll}$. Hence the protons accelerated at $t \leqslant t_{\rm coll}$ ($\sim t_{\rm rad}$) will illuminate the MCs. However, in order to interact with the cold protons inside MCs, the accelerated CR protons have to escape from the SNR shock first. The protons which have higher energies will have more probability to escape the confinement region and take part in the hadronic interaction. Protons with lower energies will not be energetic enough to escape the confinement region. Since we are considering the interaction at a time when the outermost boundary of the confinement region ($R_{\rm esc}$) collides with the MC surface ($r_{\rm MC}$), i.e., $t_{\rm coll}$, only the higher energy protons will take part in the hadronic interaction at $t_{\rm coll}$, and the lower energy protons will still be confined around the SNR. Consequently, a dominant hadronic contribution primarily in the highest energy, while a suppression in the escaped proton population in the lower energies, is expected from this scenario. This condition not only puts a constraint on the lower energy limit of the escaped proton population from the SNR shock, but also on the spectral shape of the escaped protons. The CRs with higher energies escape the confinement region and start seeping into the MC when the escaping boundary ($R_{\rm esc}$) contacts the surface of the MC ($r_{\rm MC}$) (Makino et al. 2019). The schematic diagram explaining the collision, as well as the escape of the accelerated proton population is shown in Figure 1.

To estimate the minimum energy needed to escape the SNR shock, we use a phenomenological model, where the escape energy is expected to be a decreasing function of the shock radius (Makino et al. 2019). This approach is based on the assumption that SNRs are responsible for observed CRs below the knee (Gabici et al. 2009; Ohira et al. 2012). The maximum energy of CR protons $E_{\rm max}$ is expected to increase up to the knee energy (=$10^{15.5}$ eV) until the beginning of the Sedov phase, and then it decreases from that epoch. The escape energy can be given by a phenomenological power-law

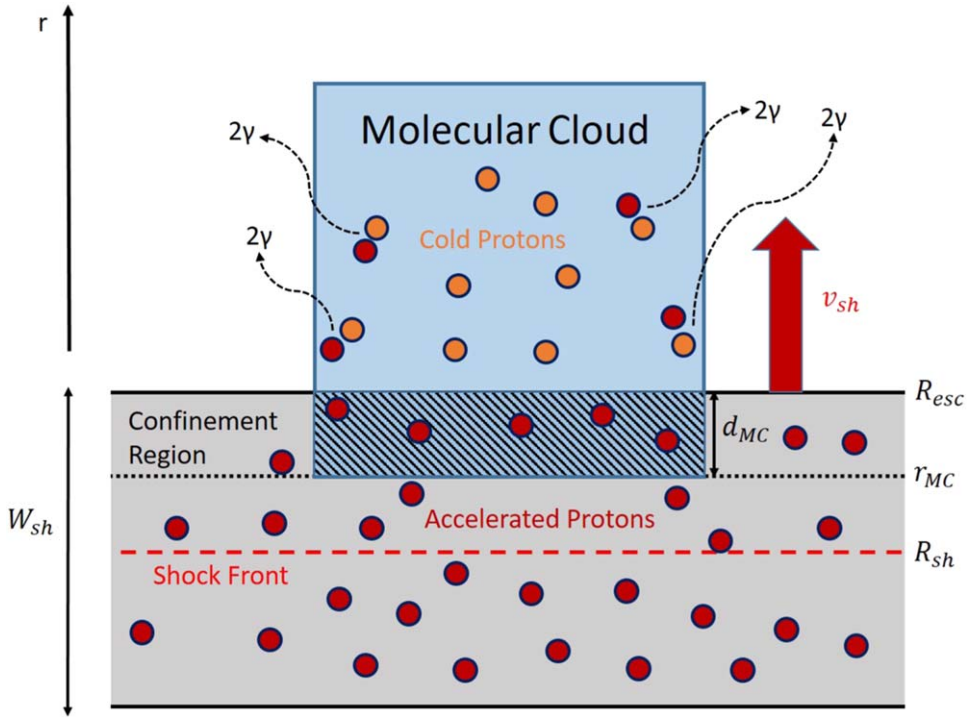

Figure 1. Schematic diagram showing the interaction between the SNR and associated MCs, following Makino et al. (2019). The radially outward direction from the cavity center is signified by the vertical axis. For the sake of simplicity, we assume that the shock front is a plane and the MC is a uniform cuboid, and the distribution of the CRs inside the cloud is one dimensional (Makino et al. 2019). The CRs have been assumed to be confined in a region around the shock front with a width of $W_{\rm sh}$, which is shown with a gray region in the figure. $R_{\rm sh}$, $r_{\rm MC}$, and $R_{\rm esc}$ signify the radius of the shock front, the distance of the surrounding MCs, and the escaping radius from the cavity center respectively. The confined region moves outward with a velocity of $v_{\rm sh}$ and the overlapped region between the MC and the confinement region is given by $d_{\rm MC}$. Part of the accelerated protons, marked with red circles escapes the confinement region through $R_{\rm esc}$, and seeps inside the MC. These escaped protons further interact with the cold protons inside the MC (marked with orange circles) and produce γ-rays.

relation,

$$E_{\rm esc} = E_{\rm max}\left(\frac{R_{\rm sh}}{R_{\rm Sedov}}\right)^{-\alpha}, \tag{4}$$

where α is a parameter describing the evolution of the maximum energy during the Sedov phase (Ohira et al. 2012; Makino et al. 2019). In this paper, we assume that $\alpha = 2$, which also dictates the suppression of escaped proton population at lower energies. Hence, assuming $E_{\rm max} = 10^{15.5}$ eV, $R_{\rm sh} = R_{\rm esc} = r_{\rm MC}$, and $R_{\rm Sedov} = 2.1$ pc, we get the minimum energy needed by the CR protons to escape from the confinement region formed around the SNR shock front, when the escape boundary contacts the surrounding MC surface, i.e., $E_{\rm esc} \approx 30$ TeV. We assume $E_{\rm esc} = E_{\rm min}$ while calculating the total hadronic contribution from the escaped CR proton population. We can also calculate the spectral index of the escaped CR proton population to ascertain its spectral shape. Since the protons are accelerated by the DSA mechanism, we assume that the CR proton spectrum at the shock front is represented by a power law $\propto {\rm E}^{-s}$. Then the spectrum of the escaped protons, i.e., the protons having an energy greater than $E_{\rm esc}$ is given by Makino et al. (2019), Ohira et al. (2012),

$$N_{\rm esc}(E) \propto E^{-[s+(\beta/\alpha)]}, \tag{5}$$

where β represents a thermal leakage model of CR injection and is given by $\beta = 3(3\text{–s})/2$. For $s = 2$, we get $\beta = 1.5$. Plugging in the value of s, α, and β in Equation (5), we get the spectral index of the escaped CR protons to be ≈ 2.75. Note that the spectral shape and the minimum energy of the escaped protons are calculated when the escape boundary hits the surface of the surrounding MCs ($t = t_{\rm coll}$).

After the collision at $t_{\rm coll}$, the shock enters the momentum conserving, radiative pressure-driven "snowplow" phase of evolution at $t > t_{\rm coll}$. Similar to Fujita et al. (2009), we can express the shock in the cloud as a shell centered on $r = |\overrightarrow{r}| = 0$, where $\overrightarrow{r}$ represents the radially outward direction from the cavity center. Furthermore, from the momentum conservation, the radius of the shocked shell $R_{\rm shell}(t)$ inside the MCs can be written as (Fujita et al. 2009),

$$\frac{4\pi}{3}[n_{\rm MC}(R_{shell}(t)^3 - R_{\rm sh}(t_{\rm coll})^3) + n_{\rm cav}R_{\rm sh}(t_{\rm coll})^3]\dot{R}_{shell}(t) = \frac{4\pi}{3}n_{\rm cav}R_{\rm sh}(t_{\rm coll})^3 v_{\rm sh}(t_{\rm coll}), \tag{6}$$

with $R_{\rm shell} = r_{\rm MC}$ at $t = t_{\rm coll}$. $n_{\rm MC} = 45\ {\rm cm}^{-3}$, is the number density of the associated MCs and $n_{\rm cav} = 1\ {\rm cm}^{-3}$ represents the number density inside the cavity, which we choose to be the same as that of the ISM. We solve Equation (6) numerically at $t > t_{\rm coll}$. We found that it takes the time $t_{\rm stop} \sim 3.3 \times 10^4$ kyr for the shell radius to reach the radius of the observed shocked shell radius of $\sim$25 pc (Yang et al. 2006), and the calculated shell velocity of the shocked shell inside the MCs was found to be $\sim$55 km s^{-1}, which is very close to the observed internal gas velocity of the clouds of 10 km s^{-1} (Yang et al. 2006). $t_{\rm stop}$, which essentially indicates the age of the SNR+MC system, agrees well with the current age of the SNR G40.5–0.5

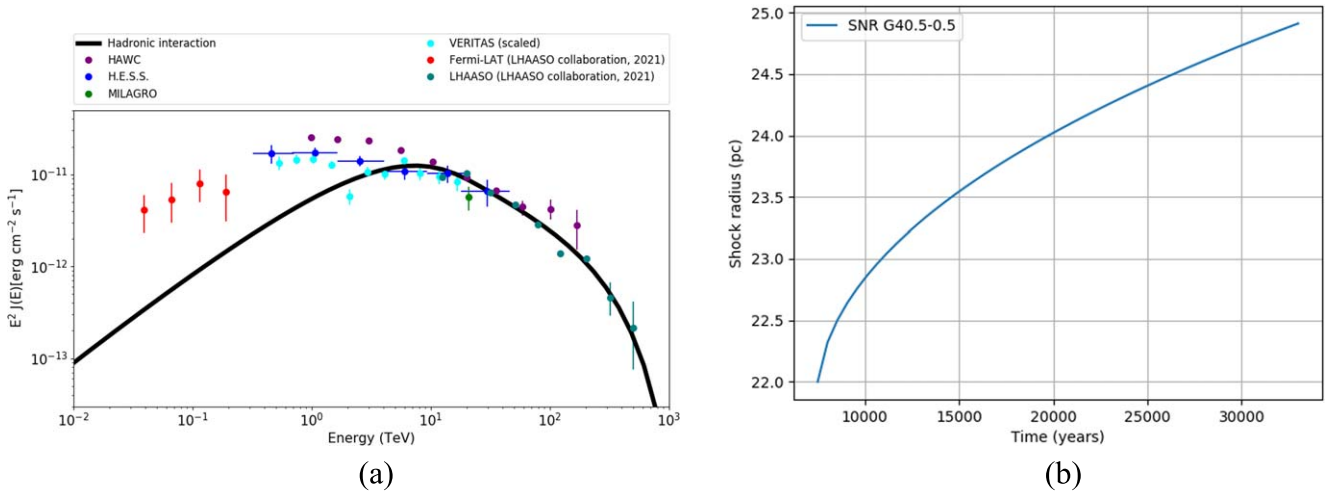

Figure 2. (a) Model γ-ray SED obtained from hadronic p–p interaction inside the MCs surrounding the SNR G40.5–0.5. Along with the calculated SED, data points obtained from Fermi-LAT (red) (Cao et al. 2021), VERITAS (cyan) (Aliu et al. 2014), H.E.S.S. (blue) (Aharonian et al. 2009), MILAGRO (green) (Abdo et al. 2007), HAWC (purple) (HAWC Collaboration et al. 2019) and LHAASO (teal) (Cao et al. 2021) are also shown. The VERITAS data points have been scaled to match that measured by the H.E.S.S. observatory. (b) Time evolution of the shocked shell associated with the SNR G40.5–0.5, inside the surrounding MCs.

(20–40 kyr), and also the shocked shell velocity agrees well with the observation. If the velocity of the shocked shell was equal to the internal gas velocity of the clouds, then no shell would have been observed. But since a shocked shell inside the surrounding MCs has been observed, it is expected for the velocity of the shell to be somewhat higher. This shows that the model is consistent with present-day observations of SNR G40.5–0.5. The variation of the shocked shell with time has been given in Figure 2(b).

Now in this work, we have assumed that escaped CR protons that have entered clouds do not escape from the clouds before they lose energy through rapid radiative cooling (Fujita et al. 2009; Makino et al. 2019). For that, the diffusion coefficient inside the MCs has to be very low compared to that observed in the ISM. Alternatively, it can be represented by the condition $t_{\rm diff} \geqslant t_{\rm stop}$, where $t_{\rm diff}$ is the diffusion time of CRs inside a cloud, and it is given by $t_{\rm diff} \sim L_{\rm MC}^2/6{\rm D(E)}$. $L_{\rm MC}$ is the size of the MCs and D(E) is the energy-dependent diffusion coefficient (Fujita et al. 2009).

From the observed secondary-to-primary ratio of CR in the Galaxy, the energy-dependent diffusion coefficient in the Galaxy has been found to be ${\rm D(E)} \approx 10^{28}\chi({\rm E}/10\,{\rm GeV})^{\delta}\,{\rm cm^2 s^{-1}}$, where δ can be between 0.3–0.6 and χ is a multiplicative factor (De Sarkar et al. 2021). It has been estimated before that although the value of χ is 1 in the Galaxy, inside dense MCs, the value is $\chi < 1$ (Gabici et al. 2009). The small value of χ can be attributed to the reduction of the diffusion coefficient by the plasma waves generated by a stream of escaping CRs near the vicinity of the SNR (Wentzel 1974; Fujita et al. 2009). In order to fulfill the condition $t_{\rm diff} \geqslant t_{\rm stop}$, we found that the value of χ must follow the condition $\chi \leqslant 0.01$ (Fujita et al. 2009). This suppression of diffusion coefficient can be easily realized inside a dense molecular cloud environment, as the value of the diffusion coefficient inside MCs is estimated to be of the order of 10^{25}–$10^{26}\,{\rm cm^2\,s^{-1}}$ (Gabici et al. 2009). If this is the case, then we can comfortably state that the injected CR protons inside the MCs lose their energy before escaping from the MCs. Moreover, since there is no effect of diffusion on the injected CR proton population, the spectral shape of the proton population does not change before they lose their energy radiatively. So we can assume the injected CR proton population attains a steady state before losing energy through hadronic p–p interaction. Thus, we calculate the total γ-ray produced from this proton population through hadronic p–p interaction, while keeping in mind that the γ-ray spectrum calculated at the present age will be the same as that calculated at $t \sim t_{\rm coll}$.

We have used GAMERA (Hahn 2016) to calculate the steady-state γ-ray spectra from the population of injected CR protons inside the MCs that surround the SNR G40.5–0.5. We have used a CR proton population having a power-law spectrum in the form of $N_p \propto E^{-\alpha_p}$, with a spectral index of $\alpha_p \approx 2.75$, a minimum energy of $E_{\rm min} \approx 30\,{\rm TeV}$, and maximum energy of $E_{\rm max} \approx 10^{15.5}\,{\rm eV}$, i.e., the knee energy. We have considered the semianalytical method developed by Kafexhiu et al. (2014) to perform the hadronic interaction calculation. The magnetic field inside the cloud was assumed to be $B_{\rm MC} \sim 60\,\mu{\rm G}$ (Fujita et al. 2009) and the number density used was $n_{\rm MC} = 45\,{\rm cm^{-3}}$ (Li et al. 2021). The total energy of the injected protons needed to fit the data observed by various observatories is $W_p \sim 2.5 \times 10^{49}\,{\rm erg}$, which is consistent with the usual 1%–10% of the kinetic energy released in SNRs ($E_{\rm SN} = 10^{51}$ erg) (Aharonian et al. 2004). The calculated spectrum, along with the observed data points are given in Figure 2(a).

From the figure, it can be seen that the γ-ray data observed by LHAASO, HAWC, H.E.S.S., and VERITAS were partially explained by the hadronic model, due to the suppression of the parent proton population at sub-TeV energies. It is also evident from the figure that an additional emission component is required for explaining the GeV–TeV part of the SED observed by Fermi-LAT, H.E.S.S., and VERITAS. Moreover, lower energy γ-ray data points (not shown in Figure 2 (a)) obtained by Li et al. (2021) could not be explained by the same hadronic model, further indicating the necessity of additional emission components. In the next section, we aim to explain the sub-TeV, as well as lower energy (0.1–10 GeV) γ-ray data points using leptonic contributions from both SNR G40.5–0.5 and the PWN associated with PSR 1907+0602.

4. Leptonic Modeling

4.1. PWN J1907+0602

Along with the hadronic contribution discussed in Section 3, we also take into account the contribution from the leptonic emission of relativistic electron population from the PWN powered by the rotation powered GeV pulsar PSR J1907 +0602. The offset between the centroid of this extended source and PSR J1907+0602 indicates that this is a relic PWN (Li et al. 2021). We have considered a steady-state relativistic electron population from this PWN and calculated the total leptonic contribution from this source.

We have considered different leptonic cooling mechanisms, such as IC, synchrotron, and bremsstrahlung (Blumenthal & Gould 1970; Ghisellini et al. 1988; Baring et al. 1999), and obtained the total γ-ray SED from the electron population associated with the PWN using GAMERA (Hahn 2016). The distance and the age of the PWN were set at 3.2 kpc and 19.5 kyr respectively (Abdo et al. 2010), the same as that of PSR J1907+0602. The value of the magnetic field associated with a PWN, in general, is low ($\sim \mu$G), due to the adiabatic expansion of the PWN with time (Martín et al. 2012). The magnetic field associated with PWN J1907+0602 was assumed to be $B_{\rm PWN} \approx 3\ \mu$G, in order to be consistent with previous works by Li et al. (2021) and Crestan et al. (2021). The number density inside the PWN was assumed to be $n_{\rm PWN} = 0.1\ {\rm cm}^{-3}$. To calculate the IC contribution from the PWN, we have considered the ISRF model from Popescu et al. (2017). We have also considered the contribution of cosmic microwave background (CMB), having the temperature $T_{\rm CMB} = 2.7$ K and energy density of $U_{\rm CMB} = 0.25\ {\rm eV\ cm}^{-3}$. The spectrum of the electron population was assumed to be a simple power law with an exponential cutoff in the form of $N_e \propto E^{-\alpha_e^{\rm PWN}} \exp(-E/E_{\rm max}^{e,{\rm PWN}})$. The spectral index of the spectrum was taken as $\alpha_e^{\rm PWN} \approx 1.5$ and the maximum energy of the population was considered to be $E_{\rm max}^{e,{\rm PWN}} \approx 10$ TeV, which is constrained by the observed X-ray upper limits. The minimum energy of the electron population $E_{\rm min}^{e,{\rm PWN}}$ was given by the rest mass energy. The energy budget of this relativistic electron population needed to satisfy the observed VHE data was found to be $W_e^{\rm PWN} \sim 7.5 \times 10^{47}$ erg.

4.2. SNR G40.5–0.5

An extended object, labeled Fermi J1906+0626, illuminated in the GeV γ-ray range, was reported from the off-pulse phase-resolved analysis done by Li et al. (2021). In their work, the spectrum of this extended object, bright in the lower energy, was described by hadronic interaction between the SNR+MC system, modified by the diffusion inside the clouds. However, in this work, we consider that the lower energy spectrum is due to the contribution from the electrons escaped from the shock front of SNR G40.5–0.5, a scenario that has not been explored in previous works. The escaped electron population from the confinement region around the shock gets injected inside the surrounding MCs, and then interacts with the ambient medium of the same MCs. Emission is produced through synchrotron (Blumenthal & Gould 1970; Ghisellini et al. 1988) and IC (Blumenthal & Gould 1970) cooling of the injected electron population. Since the number density of the MCs is much higher compared to that of ISM, bremsstrahlung emission (Baring et al. 1999) dominates the lower energy γ-ray SED. We have used GAMERA (Hahn 2016) as before, to calculate the leptonic emissions.

Since the electrons go through the same evolution process as the protons before escaping from the SNR shock front, we assume that the spectral index of escaped CR electrons is the same as that of the protons (Ohira et al. 2012), i.e., $\alpha_e^{\rm SNR} \approx 2.75$. However, since the electrons, being leptons, lose energy radiatively very fast compared to protons, we have considered a simple power law with the exponential cutoff as the spectrum of the runaway electron population in the form of $N_e \propto E^{-\alpha_e^{\rm SNR}} \exp(-E/E_{\rm max}^{e,{\rm SNR}})$. The maximum energy associated with the runaway electron population spectrum is given by the relation (Yamazaki et al. 2006; Fujita et al. 2009),

$$E_{\rm max}^{e,{\rm SNR}} = 14 h^{-1/2} \left(\frac{v_{\rm sh}}{10^8\ {\rm cm/s}}\right)\left(\frac{B}{10\ \mu G}\right)^{-1/2} {\rm TeV} \qquad (7)$$

where h($\sim$1) is determined by the shock angle and the gyro-factor, $v_{\rm sh}$ is the velocity of the shock front and B is the downstream magnetic field. Since we calculate the maximum energy of the lepton population at the collision time, we considered $v_{\rm sh}(t_{\rm coll})$ as velocity in the above relation. We consider the magnetic field ($B_{\rm MC}$) and number density ($n_{\rm MC}$) inside the MCs the same as that considered in Section 3, so we use $B = B_{\rm MC}$ in the above relation. The minimum energy of the electron population was assumed to be $E_{\rm min}^{e,{\rm SNR}} = 500$ MeV. For the IC contribution, we have adopted the interstellar radiation field (ISRF) modeled in Popescu et al. (2017) at the position of SNR G40.5–0.5. The CMB contribution was also taken into account. The necessary energy budget of the runaway electron population to explain the lower energy γ-ray SED was found to be $W_e^{\rm SNR} \sim 1 \times 10^{49}$ erg.

After considering synchrotron, IC, and bremsstrahlung contributions from the runaway electron population from SNR G40.5–0.5, the lower energy (0.1–10 GeV) γ-ray SED was obtained by Li et al. (2021), could be explained adequately. The dominant contribution in explaining the SED in the 0.1–10 GeV range, came from the bremsstrahlung component, which is expected, as the morphology associated with this lower energy γ-ray emission was found to be spatially coincident with the molecular material enhancement observed inside the dense clumps surrounding SNR G40.5–0.5. The IC contribution was rather negligible in this case. The necessary model parameters used in this work have been summarized in Table 1.

The MWL SED of the source LHAASO J1908+0621 is shown in Figure 3, along with calculated SEDs from various leptonic and hadronic contributions from SNR G40.5–0.5 and PWN J1907+0602. From the figure, it can be seen that the total model flux satisfies the observed γ-ray SED data points, from lower energies to the VHE–UHE regime. Most notably, the UHE γ-ray spectrum, observed by LHAASO can be explained by the hadronic component from the SNR+MC system. Fermi-LAT data points above 30 GeV, as obtained by Li et al. (2021), as well as Cao et al. (2021), were explained by the leptonic contribution from the PWN, which also conforms with the Fermi-LAT morphology map obtained by Li et al. (2021; see Figure 2 of that paper). Moreover, both PWN J1907+0602 and the SNR+MC system contribute to explaining the γ-ray SED observed by VERITAS and H.E.S.S. The bremsstrahlung emission from the escaped electron population associated with

Table 1
Parameters Used in The Model

Source	Component	Parameter	Value
SNR G40.5–0.5 + MCs	Hadronic	Injection spectral index (α_p)	2.75
		Minimum energy ($E_{\rm min}$)	30 TeV
		Maximum energy ($E_{\rm max}$)	3.2 PeV
		Energy budget (W_p)	2.5×10^{49} erg
		Magnetic field ($B_{\rm MC}$)	60 μG
		Number density ($n_{\rm MC}$)	45 cm^{-3}
	Leptonic	Injection spectral index ($\alpha_e^{\rm SNR}$)	2.75
		Minimum energy ($E_{\rm min}^{e,\rm SNR}$)	500 MeV
		Maximum energy ($E_{\rm max}^{e,\rm SNR}$)	6.9 TeV (Equation (7))
		Energy budget ($W_e^{\rm SNR}$)	1×10^{49} erg
		Magnetic field ($B_{\rm MC}$)	60 μG
		Number density ($n_{\rm MC}$)	45 cm^{-3}
PWN J1907+0602	Leptonic	Injection spectral index ($\alpha_e^{\rm PWN}$)	1.5
		Minimum energy ($E_{\rm min}^{e,\rm PWN}$)	0.511 MeV
		Maximum energy ($E_{\rm max}^{e,\rm PWN}$)	10 TeV
		Energy budget ($W_e^{\rm PWN}$)	7.5×10^{47} erg
		Magnetic field ($B_{\rm PWN}$)	3 μG
		Number density ($n_{\rm PWN}$)	0.1 cm^{-3}

SNR G40.5–0.5, also satisfies the lower energy γ-ray SED. Very crucially, the combined synchrotron emission obtained from our model satisfies all of the upper limits obtained from various XMM-Newton data analyses (Li et al. 2021; Crestan et al. 2021; Pandel 2015), further confirming the validity of our model.

As can be seen from the upper panel of Figure 3, there remains a discrepancy between the data obtained by the Imaging Atmospheric Cherenkov Telescope (IACT) experiments and HAWC in the energy band of 1 to 10 TeV. Since HAWC has observed a larger source extent (HAWC Collaboration 2019), the data observed by both H.E.S.S. and VERITAS are inconsistent with that observed by HAWC (Crestan et al. 2021). Consequently, in this particular work, we have tried to fit the data in this important band of 1–10 TeV, by favoring the HAWC data over the IACT data. The corresponding residual, i.e., (data-model)/error, the plot is given in the lower panel of Figure 3. From the figure, it can be clearly seen that the total model SED is more consistent with the HAWC data, as compared to the data observed by H.E.S.S. and VERITAS in the 1–10 TeV range.

5. Neutrino Flux

Neutrinos are also produced in hadronic p–p interactions, along with γ-rays. Consequently, if there are γ-ray sources that are powered by hadronic interactions, neutrino emission from the same source region is also expected. MGRO J1908+06, the MILAGRO counterpart of LHAASO J1908+0621, may be a neutrino source due to its extended nature and hard TeV γ-ray spectrum (Gonzalez-Garcia et al. 2009; Halzen et al. 2017). IceCube neutrino telescope searched for point-like source emission in the vicinity of this source. The astrophysical muon neutrino flux observed from this source region, has been found to have the second-best p-value, being a Galactic source (Aartsen et al. 2019a). However, the emission is still consistent with the background. Although not quite significant yet, the presence of a neutrino hotspot associated with the source indicates hadronic emission in the highest energy range. The hadronic p–p interaction considered in the SNR+MC system to explain the UHE γ-rays observed by LHAASO, also produces neutrinos in the source region. In this section, we calculate the total muonic neutrino flux produced from the interactions between the escaped CR parent proton population from the SNR G40.5–0.5 and the cold protons residing inside the surrounding MCs.

To calculate the flux of the muonic neutrinos $\nu_\mu + \tilde{\nu}_\mu$, we use the semianalytical formulation developed by Kelner et al. (2006). Following Kelner et al. (2006), we have included the muonic neutrinos produced from direct decay of charged pions ($\pi \rightarrow \mu\ \nu_\mu$) labeled as $\nu_\mu^{(1)}$ and from the decay of muons ($\mu \rightarrow$ e $\nu_\mu\ \nu_e$) labeled as $\nu_\mu^{(2)}$. E_p and E$_\nu$ denote the energies of the proton population and produced neutrinos respectively. The total neutrino production rate from inelastic hadronic p–p interaction can be calculated using the equation (Kelner et al. 2006),

$$\Phi_\nu(E_\nu) = \frac{cn_{\rm MC}}{4\pi d^2} \int \sigma_{\rm inel}(E_\nu/x) J_p(E_\nu/x) F_\nu(x, E_\nu/x) \frac{dx}{x} \quad (8)$$

where the variable $x = E_\nu/E_p$, c is the velocity of light, $n_{\rm MC}$ is the density of the molecular clouds, $d(= 8$ kpc) is the distance of the SNR+MC system, $\sigma_{\rm inel}(E_p)$ is the inelastic cross section of p–p interaction, which is given by,

$$\sigma_{\rm inel}(E_p) = 34.3 + 1.88L + 0.25L^2 \text{ mb} \quad (9)$$

where $L = \ln(E_p/1$ TeV). $J_p(E_p)$ signifies the spectrum of the parent proton population and it is given by $J_p(E_p) = {\rm A}(E_p/1\ {\rm TeV})^{-\alpha_p}$. The normalization A (in the unit of erg^{-1}) can be calculated by performing the integration $W_p = A \int_{E_{\rm min}}^{E_{\rm max}} E_p\ (E_p/1\ {\rm TeV})^{-\alpha_p}\ dE_p$, where the integration parameters are the same as that discussed in Section 3. The condition that the maximum energy of the parent proton population can reach up to $E_{\rm max} \approx 10^{15.5}$ eV, is taken into account while considering the proton spectrum. F_ν represents the function that explains the spectra of $\nu_\mu^{(1)}$ and $\nu_\mu^{(2)}$, which get produced from the decays of charged pions and muons respectively (Kelner et al. 2006). Note that while for $\nu_\mu^{(2)}$, the lower and upper integration limits for Equation (8) are 0 and 1 respectively, for $\nu_\mu^{(1)}$, the upper

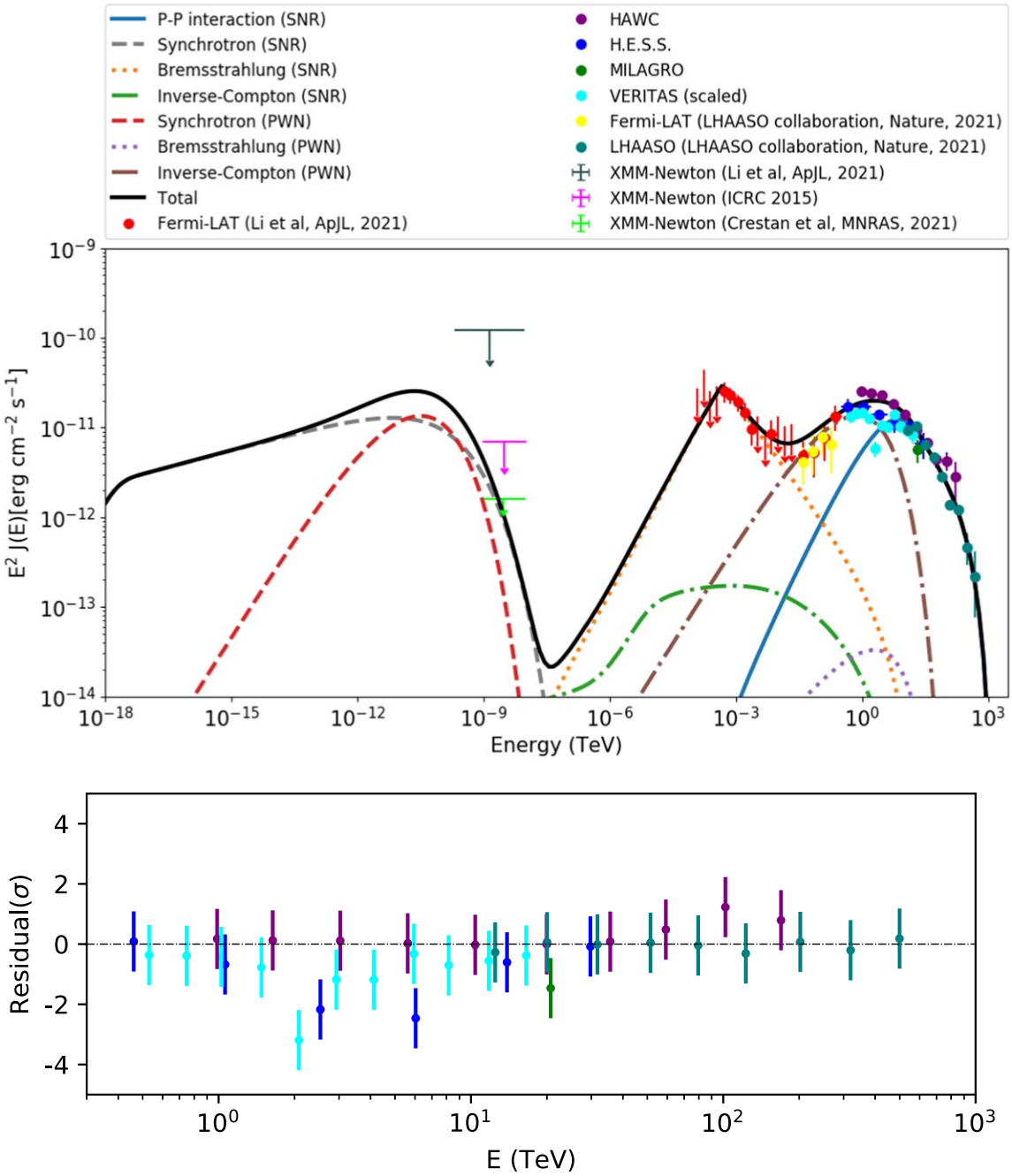

Figure 3. Upper panel: MWL SED of LHAASO J1908+0621. Data points obtained from different observations by Fermi-LAT (red Li et al. 2021, yellow Cao et al. 2021), HAWC (purple) (HAWC Collaboration et al. 2019), H.E.S.S. (blue) (Aharonian et al. 2009), MILAGRO (green) (Abdo et al. 2007), VERITAS (cyan) (Aliu et al. 2014) and LHAASO (teal) (Cao et al. 2021) are shown in the figure. The VERITAS data points have been scaled to match that measured by the H.E.S.S. observatory. The XMM-Newton upper limit obtained from Li et al. (2021) is shown in dark grey. XMM-Newton upper limits obtained from Crestan et al. (2021) and Pandel (2015) are shown in lime and magenta respectively. The solid blue line corresponds to the hadronic component from SNR G40.5–0.5. The synchrotron (gray dashed), bremsstrahlung (orange dotted), and IC (light green dotted–dashed) components from SNR G40.5–0.5 are shown. Also, synchrotron (red dashed), bremsstrahlung (violet dotted), and IC (brown dotted–dashed) components from PWN J1907+0602 are shown. The total combination of all of these components is shown with a black solid line. Lower panel: the corresponding residual plot for the fit of the total model SED to the observed data from different observatories. The color scheme of the data points is the same as that described in the upper panel.

limit is 0.427. This is because the spectrum of $F_{\nu_\mu^{(1)}}$ sharply cuts off at $x = 0.427$ (Kelner et al. 2006). By integrating Equation (8) with appropriate limits, we get the total muonic neutrino flux $\nu_\mu + \tilde{\nu}_\mu$, obtained from both channels of decays, and it is given by $\Phi_{\nu_\mu+\tilde{\nu}_\mu} = \Phi_{\nu_\mu^{(1)}+\tilde{\nu}_\mu^{(1)}} + \Phi_{\nu_\mu^{(2)}+\tilde{\nu}_\mu^{(2)}}$. Our estimated muon neutrino flux is shown in Figure 4 along with the IceCube-Gen2 sensitivity limit (Aartsen et al. 2019b).

From Figure 4, it can be seen that the model neutrino flux exceeds the sensitivity limit of IceCube-Gen2. This implies that if the hadronic component from the SNR+MC system contributes to the total observed emission from the direction of LHAASO J1908+0621 in the TeV–PeV range, then the corresponding neutrino flux will be detectable by IceCube below PeV energies. This is an important differentiator between the leptonic and hadronic scenarios in the UHE range,

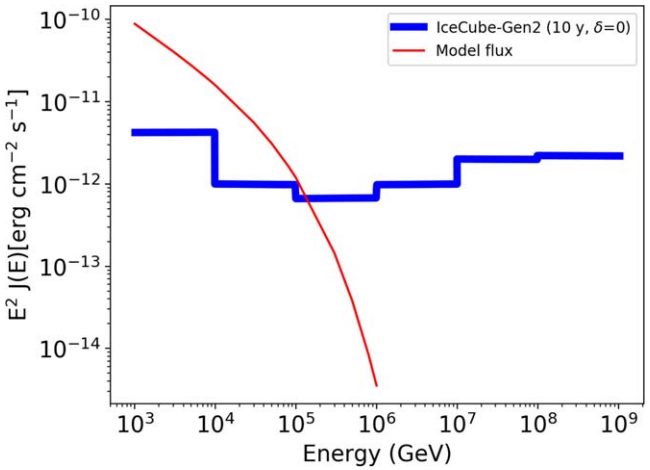

Figure 4. The estimated total muonic neutrino flux reaching the Earth from SNR G40.5–0.5. The red continuous line represents the total muonic neutrino flux produced due to the interactions of the escaped CR protons from SNR G40.5–0.5 with the cold protons in the associated molecular clouds. The blue solid dashed line indicates the sensitivity of IceCube-Gen2 to detect the neutrino flux from a point source at the celestial equator with an average significance of 5σ after 10 years of observations.

as no neutrinos would get produced if the UHE γ-ray emission from the LHAASO source is due to the IC cooling of one-zone or two-zone leptonic population (HAWC Collaboration et al. 2022). Future observations by IceCube will help to confirm the exact nature of LHAASO J1908+0621.

6. Discussion

In earlier literature (Abdo et al. 2010; Li et al. 2021), it has been posited that the multi-TeV, VHE–UHE γ-ray data points are most likely represented entirely by the leptonic emission from a population of relativistic electrons associated with the PWN of PSR J1907+0602. Li et al. (2021) have explained the VHE–UHE γ-ray data points with the leptonic component from the PWN, since the spectrum measured by Cherenkov instruments resembles the spectral signature associated with IC emission from GeV/TeV PWNe. This approach was also considered in Crestan et al. (2021), as well as in HAWC Collaboration et al. (2022). However, Crestan et al. (2021) disfavored a one-zone leptonic scenario to explain the VHE–UHE γ-ray spectra by the spatial morphology of the multi-TeV emission. The multi-TeV emission region associated with the PWN extends far from the pulsar position, but the emission itself does not show any signatures of spectral softening with the distance from the pulsar, as is expected from the cooling of electrons (Crestan et al. 2021). Moreover, due to the Klein–Nishina suppression of the IC cross section at higher energies, the maximum energy of the electron population will attain a large value, in order to fit the observed VHE–UHE γ-ray data entirely by a one-zone electron population from PWN J1907+0602. Furthermore, if the multi-TeV, VHE–UHE γ-ray data points were explained with a one-zone leptonic model from PWN J1907+0602, then the corresponding synchrotron flux would be incompatible with the X-ray upper limits obtained by Crestan et al. (2021); Pandel (2015) in the keV energy range. These issues were echoed in HAWC Collaboration et al. (2022), in which the authors also favored a two population scenario to explain the VHE–UHE γ-ray emission. Note that Crestan et al. (2021) also explored a one-zone hadronic model to explain the VHE–UHE γ-rays and found that a very hard photon index is needed in their model, which was not seen in other TeV sources associated with SNRs. Hence, they concluded that a fully hadronic model is also disfavored. HAWC Collaboration et al. (2022) also stated that a one-zone hadronic model to explain the UHE γ-rays observed by HAWC is not favored due to the lack of sufficient energy to power the hadronic emission and fit the observed data. It is clear that in order to explain the VHE–UHE γ-ray emission, a two population model is required. Any one-zone leptonic, as well as the hadronic scenario, is not sufficient for explaining the MWL SED of LHAASO J1908+0621 consistently.

In this paper, we explore a lepto-hadronic scenario of CR interaction to produce VHE–UHE γ-rays observed from the direction of LHAASO J1908+0621, with a particular focus on proper hadronic modeling required to explain both UHE γ-rays observed by LHAASO, as well as the neutrino hotspot coincident with the source position, detected by ICECUBE. We have considered that the emission in the 10 GeV–10 TeV energy range has originated due to the leptonic emission from PWN J1907+0602, whereas above 10 TeV, the emission has a hadronic origin. We use a physically viable and detailed model of CR interaction inside an SNR+MC system (Fujita et al. 2009; Ohira et al. 2012; Makino et al. 2019) to partially explain the observed UHE γ-ray data points. The choice of the free parameter α constrains the minimum energy and the spectrum of the escaped CR proton population, which consistently reproduces the γ-ray SED in the multi-TeV energy range. Moreover, the model matches the present-day observation of the state of the shocked shell inside the MCs. In addition, we have also included emission due to leptonic cooling from PWN J1907+0602. Finally, we have shown that by considering these two scenarios, the γ-ray data points extending from 10 GeV to 1 PeV, can be explained well.

Li et al. (2021) had shown previously that in the 0.1–10 GeV range, an extended source, Fermi J1906+0626, is present overlapping the source region of MGRO J1908+06. The authors had described SED from this source by a soft spectrum, which is similar to the ones observed in evolved SNRs. Moreover, they reported that from the Fermi-LAT analysis of this extended source, a significant peak was found coinciding with an enhancement of molecular cloud material, thus justifying the tentative hadronic origin of this low energy component. They further fitted the SED with a steep power-law proton spectrum, which is modified by diffusion. The same model was considered in HAWC Collaboration et al. (2022), where lower energy data points were fitted by a hadronic component from the SNR+MC system. However, in this work, we explain the γ-ray SED in the 0.1–10 GeV range, with leptonic contribution from the SNR G40.5–0.5 and its surrounding MC system. We considered a power-law spectrum with an exponential cutoff to explain the relativistic electron population associated with the SNR+MC system. We considered that, like protons, electrons could also escape from the confinement region around the shock front of the SNR, and get injected into the MCs. After considering various leptonic cooling mechanisms inside the MCs, we found that the leptonic component from SNR G40.5–0.5 is adequate to explain the lower energy γ-ray emission. Since bremsstrahlung emission dominates the IC cooling inside a dense molecular medium, it was primarily used to explain the lower energy γ-ray SED. Moreover, this emission scenario was also corroborated by the spatial morphology observed by Fermi-LAT (Li et al. 2021).

The combined lepto-hadronic scenario explored in our model not only satisfactorily explains the observed γ-ray SED from low- to ultra-high energy, but the synchrotron emission obtained from our model is also consistent with the observed X-ray upper limits.

Since there is a possibility of an IceCube neutrino hotspot present in the source region, we also calculated the total muonic neutrino flux from the hadronic interaction considered in this paper. If the UHE emission is due to leptonic emission, then no neutrino would be seen from the source region. Although the hotspot is not significant yet, as observed by previous generation IceCube, the IceCube-Gen2 has better sensitivity for detecting neutrino from a Galactic source. From our calculation, we found that the total neutrino flux exceeds the sensitivity limit of IceCube-Gen2, which implies that if the emission from LHAASO J1908+0621 is partially hadronic in origin, then IceCube-Gen2 will be able to detect neutrino from the source region. Future observation by IceCube will be crucial to dividing the two emission contributions from the SNR+MC system and the PWN currently considered.

Although the model explored in this paper satisfies the observed γ-ray data points, as well as the X-ray upper limits, a lot of issues are still needed to be clarified by future experiments in the MWL bands. Since the source region is very complex, with the PWN and the SNR+MC system juxtaposed within the 68% containment region of many observatories, further morphological observations are very crucial to better constrain the model. More detailed morphological observations in the UHE γ-ray regime, which we expect that Cherenkov Telescope Array (CTA) will provide in the near future, will be important in discerning the source localizations as well as their contributions. Moreover, long-term X-ray and radio observations are very crucial to constrain the modeling of this source. X-ray and radio observations will not only constrain the magnetic field, but will also affect the minimum energy, the injection spectral index, and the energy budget of the parent lepton population of both the PWN and SNR+MC systems. Furthermore, astrophysical neutrino detection at the source region will in turn confirm the contribution of the hadronic component from the SNR+MC system at the UHE regime.

7. Conclusion

In conclusion, in this paper, we have studied the underlying emission mechanism of LHAASO J1908+0621 suggested by the observed data, and subsequently explored a simple, analytical, phenomenological model that is compatible with the MWL data points hitherto observed. In our model, the leptonic component from PWN J1907+0602 is dominant in the 10 GeV to 10 TeV range, whereas the hadronic component is used to explain the observed UHE SED above the 10 TeV to 1 PeV energy range. The leptonic contribution from the SNR +MC system explains the lower energy part (0.1–10 GeV) of the γ-ray SED. Our model also satisfies the observed X-ray upper limits. However, as discussed earlier, more detailed observations about the γ-ray emitters in energy ranges from 0.5 TeV to 1 PeV, will reveal more insight into the complex source region in the short future. Additionally, the crucial observations in X-ray and radio bands will play a huge role in unveiling the radiation mechanism of this source region through detailed MWL analyses. Future observations by the CTA observatory, as well as neutrino observation by IceCube-Gen2 at the source position, will be important to untangle the exact nature of this enigmatic source in both low and high energies.

The authors thank the anonymous reviewer for constructive criticism and useful suggestions regarding the manuscript. A.D. S. thanks Maheswar Swar for help regarding Figure 1.

Software: GAMERA (https://github.com/libgamera/GAMERA).

ORCID iDs

Agnibha De Sarkar https://orcid.org/0000-0001-6047-6746
Nayantara Gupta https://orcid.org/0000-0002-1188-7503

References

Aartsen, M. G., Ackermann, M., Adams, J., et al. 2019a, EPJC, 79, 234
Aartsen, M. G., Ackermann, M., Adams, J., et al. 2019b, arXiv:1911.02561
Aartsen, M. G., Ackermann, M., Adams, J., et al. 2020, PhRvL, 124, 051103
Abdalla, H., Abramowski, A., Aharonian, F., et al. 2018, A&A, 612, A1
Abdo, A. A., Allen, B., Berley, D., et al. 2007, ApJ, 664, L91
Abdo, A. A., Ackermann, M., Ajello, M., et al. 2010, ApJ, 711, 64
Abdollahi, S., Acero, F., Ackermann, M., et al. 2020, ApJS, 247, 33
Akhperjanian, F. A., Aharonian, A. G., Anton, G., et al. 2009, A&A, 499, 723
Aharonian, F. A., Akhperjanian, A. G., Aye, K. M., et al. 2004, Natur, 432, 75
Aliu, E., Archambault, S., Aune, T., et al. 2014, ApJ, 787, 166
Baring, M. G., Ellison, D. C., Reynolds, S. P., Grenier, I. A., & Goret, P. 1999, ApJ, 513, 311
Bartoli, B., Bernardini, P., Bi, X. J., et al. 2012, ApJ, 760, 110
Blumenthal, G. R., & Gould, R. J. 1970, RvMP, 42, 237
Cao, Z. 2010, ChPhC, 34, 249
Cao, Z., Aharonian, F. A., An, Q., et al. 2021, Natur, 594, 33
Case, G. L., & Bhattacharya, D. 1998, ApJ, 504, 761
Crestan, S., Giuliani, A., Mereghetti, S., et al. 2021, MNRAS, 505, 2309
De Naurois, M. 2019, ICRC (Madison, WI), 358, 656
De Sarkar, A., Biswas, S., & Gupta, N. 2021, JHEAp, 29, 1
Downes, A. J. B., Pauls, T., & Salter, C. J. 1980, A&A, 92, 47
Duvidovich, L., Petriella, A., & Giacani, E. 2020, MNRAS, 491, 5732
Fujita, Y., Ohira, Y., Tanaka, S. J., & Takahara, F. 2009, ApJL, 707, L179
Gabici, S., Aharonian, F. A., & Casanova, S. 2009, MNRAS, 396, 1629
Galante, N. 2012, in AIP Conf. Ser., 1505, High Energy Gamma-Ray Astronomy: 5th Int. Meeting on High Energy Gamma-Ray Astronomy, ed. F. A. Aharonian, W. Hofmann, & F. M. Rieger (Melville, NY: AIP), 202
Ghisellini, G., Guilbert, P. W., & Svensson, R. 1988, ApJL, 334, L5
Gonzalez-Garcia, M. C., Halzen, F., & Mohapatra, S. 2009, APh, 31, 437
Hahn, J. 2016, ICRC (The Hague), 236, 917
Halzen, F., Kheirandish, A., & Niro, V. 2017, APh, 86, 46
HAWC Collaboration, Abeysekara, A. U., Albert, A., et al. 2019, PhRvL, in press, arXiv:1909.08609
HAWC Collaboration, Albert, A., Alfaro, R., et al. 2022, ApJ, 928, 116
H.E.S.S. Collaboration, Abramowski, A., Aharonian, F., et al. 2016, Natur, 531, 476
H.E.S.S. Collaboration, Abdalla, H., Abramowski, A., et al. 2018, A&A, 612, A9
Kafexhiu, E., Aharonian, F., Taylor, A. M., & Vila, G. S. 2014, PhRvD, 90, 123014
Kelner, S. R., Aharonian, F. A., & Bugayov, V. V. 2006, PhRvD, 74, 034018
Li, J., Liu, R.-Y., de Oña Wilhelmi, E., et al. 2021, ApJL, 913, L33
Lyne, A. G., Stappers, B. W., Bogdanov, S., et al. 2017, ApJ, 834, 137
MAGIC Collaboration, Acciari, V. A., Ansoldi, S., et al. 2020, A&A, 642, A190
Makino, K., Fujita, Y., Nobukawa, K. K., Matsumoto, H., & Ohira, Y. 2019, PASJ, 71, 78
Martín, J., Torres, D. F., & Rea, N. 2012, MNRAS, 427, 415
Ohira, Y., Murase, K., & Yamazaki, R. 2011, MNRAS, 410, 1577
Ohira, Y., Yamazaki, R., Kawanaka, N., & Ioka, K. 2012, MNRAS, 427, 91
Pandel, D. 2015, ICRC (The Hague), 34, 743
Popescu, C. C., Yang, R., Tuffs, R. J., et al. 2017, MNRAS, 470, 2539
Stil, J. M., Taylor, A. R., Dickey, J. M., et al. 2006, AJ, 132, 1158
Wentzel, D. G. 1974, ARA&A, 12, 71
Yamazaki, R., Kohri, K., Bamba, A., et al. 2006, MNRAS, 371, 1975
Yang, J., Zhang, J.-L., Cai, Z.-Y., Lu, D.-R., & Tan, Y.-H. 2006, ChJAA, 6, 210